

A spectral line survey of Orion KL in the bands 486–492 and 541–577 GHz with the Odin[★] satellite^{★★}

I. The observational data

A. O. H. Olofsson^{1,2}, C. M. Persson¹, N. Koning³, P. Bergman^{1,4}, P. F. Bernath^{5,6,7}, J. H. Black¹, U. Frisk⁸,
W. Geppert⁹, T. I. Hasegawa^{3,10}, Å. Hjalmarsen¹, S. Kwok^{3,11}, B. Larsson¹², A. Lecacheux¹³, A. Nummelin¹⁴,
M. Olberg¹, Aa. Sandqvist¹², and E. S. Wirström¹

¹ Onsala Space Observatory (OSO), 43992 Onsala, Sweden

e-mail: henrik@oso.chalmers.se

² LERMA, Observatoire de Paris, 61 Av. de l'Observatoire, 75014 Paris, France

³ Department of Physics and Astronomy, University of Calgary, Calgary, AB T2N 1N4, Canada

⁴ European Southern Observatory, Alonso de Cordova 3107, Vitacura, Casilla 19001, Santiago, Chile

⁵ Department of Chemistry, University of Arizona, Tucson, AZ 85721, USA

⁶ Department of Chemistry, University of Waterloo, Waterloo, ON N2L 3G1, Canada

⁷ Department of Chemistry, University of York, Heslington, York YO10 5DD, UK

⁸ Swedish Space Corporation, PO Box 4207, 17104 Solna, Sweden

⁹ Molecular Physics Division, Department of Physics, Stockholm University AlbaNova, 10691 Stockholm, Sweden

¹⁰ Institute of Astronomy and Astrophysics, Academia Sinica, PO Box 23-141, Taipei 106, Taiwan, R.O.C.

¹¹ Department of Physics, University of Hong Kong, Hong Kong, PR China

¹² Stockholm Observatory, AlbaNova University Center, 10691 Stockholm, Sweden

¹³ LESIA, Observatoire de Paris, Section de Meudon, 5 place Jules Janssen, 92195 Meudon Cedex, France

¹⁴ Computer science and engineering, Chalmers University of Technology, 41296 Göteborg, Sweden

Received 2 February 2007 / Accepted 30 August 2007

ABSTRACT

Aims. Spectral line surveys are useful since they allow identification of new molecules and new lines in uniformly calibrated data sets. The subsequent multi-transition analysis will provide improved knowledge of molecular abundances, cloud temperatures and densities, and may also reveal previously unsuspected blends of molecular lines, which otherwise may lead to erroneous conclusions. Nonetheless, large portions of the sub-millimetre spectral regime remain unexplored due to severe absorptions by H₂O and O₂ in the terrestrial atmosphere. The purpose of the measurements presented here is to cover wavelength regions at and around 0.55 mm – regions largely unobservable from the ground.

Methods. Using the Odin astronomy/aeronomy satellite, we performed the first spectral survey of the Orion KL molecular cloud core in the bands 486–492 and 541–576 GHz with rather uniform sensitivity (22–25 mK baseline noise). Odin's 1.1 m size telescope, equipped with four cryo-cooled tuneable mixers connected to broad band spectrometers, was used in a satellite position-switching mode. Two mixers simultaneously observed different 1.1 GHz bands using frequency steps of 0.5 GHz (25 h each). An on-source integration time of 20 h was achieved for most bands. The entire campaign consumed ~1100 orbits, each containing one hour of serviceable astro-observation.

Results. We identified 280 spectral lines from 38 known interstellar molecules (including isotopologues) having intensities in the range 80 to 0.05 K. An additional 64 weak lines remain unidentified. Apart from the ground state rotational 1_{1,0}–1_{0,1} transitions of *ortho*-H₂O, H₂¹⁸O and H₂¹⁷O, the high energy 6_{2,4}–7_{1,7} line of *para*-H₂O ($E_u = 867$ K) and the HDO(2_{0,2}–1_{1,1}) line have been observed, as well as the 1₀–0₁ lines from NH₃ and its rare isotopologue ¹⁵NH₃. We suggest assignments for some unidentified features, notably the new interstellar molecules ND and SH⁻. Severe blends have been detected in the line wings of the H₂¹⁸O, H₂¹⁷O and ¹³CO lines changing the true linewidths of the outflow emission.

Key words. ISM: individual: objects: Orion KL – ISM: lines and bands – ISM: molecules – line: identification – submillimeter – surveys

1. Introduction

Being the most popular target for spectral line surveys, in the Orion KL position OMC-1 has been the focal point of at least ~20 observational efforts in the mm and submm bands over the last 20 years, starting with Johansson et al. (1984, 1985), and in the frequency range 72–91 GHz. White et al. (2003) provide an extensive list of this earlier work in their introduction. Using the James Clerk Maxwell Telescope (JCMT),

* Odin is a Swedish-led satellite project funded jointly by the Swedish National Space Board (SNSB), the Canadian Space Agency (CSA), the National Technology Agency of Finland (Tekes), and the Centre National d'Études Spatiales (CNES, France). The Swedish Space Corporation (SSC) was the industrial prime contractor and is also responsible for the satellite operation.

** Appendix B is only available at electronic form at <http://www.aanda.org>

White et al. (2003) surveyed the bands 455–469 and 492–507 GHz, surrounding the lowest frequency range of our Odin spectral scan (486–492 GHz). The frequency range 607–725 GHz, just above the Odin spectral scan band 542–576 GHz, has been surveyed by Schilke et al. (2001) using the Caltech Submillimeter Observatory (CSO).

More recent additions include 159.7–164.7 GHz (Lee & Cho 2002), 795–903 GHz (Comito et al. 2005), 260–328 GHz (Yoshida & Phillips IAU 231¹), and an IRAM 30 m survey (168 GHz in three windows between 80 and 281 GHz) by Tercero et al. (IAU 231¹).

The first imaging line survey of Orion KL in the submm range (337.2–339.2 and 347.2–349.2 GHz) was recently reported by Beuther et al. (2005), who used the Submillimeter Array interferometer. They later employed the same instrument to make measurements around 680 and 690 GHz with similar bandwidths (Beuther et al. 2006).

The luminous Orion Kleinmann-Low infrared nebula (Orion KL; $L \approx 10^5 L_\odot$), and its surrounding molecular cloud, is the nearest (distance of 450 pc) and probably most studied massive star formation region in the sky. A very useful review has been written by Genzel & Stutzki (1989); for reference updates see e.g., Olofsson et al. (2003), and Wiström et al. (2006). Here we summarise some source component designations and dynamical properties particularly relevant to the molecular line identification work in the current presentation of our Odin spectral scan data, which includes our molecular line assignments (in the Online Table 6).

Odin’s circa 126'' antenna beam is centred on the most prominent infrared “point” source in the KL nebula, IRc 2 (RA 05^h35^m14^s.36, Dec. –05°22'29".6 (J2000)). The Orion *hot core* source, with a size of only $\approx 10''$ and centred only 2'' S of IRc 2, is a warm (≈ 200 K, or even higher; cf. Sempere et al. 2000), dense ($\approx 10^7$ cm⁻³) clump or rather collection of clumps, characterised by a spectral line width of 5–15 km s⁻¹ centred on $v_{\text{LSR}} = 3$ –6 km s⁻¹ and exhibiting emission from nitrogen-containing species at markedly enhanced abundances. The outflowing gas, or the *plateau source*, with a size of 40–60'', may be characterised in terms of a bipolar *high-velocity flow* elongated in the SE-NW direction (reaching velocities of ± 100 km s⁻¹), and a SW-NE extended *low-velocity flow* (the “18 km s⁻¹ flow”) of size 15–30'', centred on 10 and 5 km s⁻¹, respectively. Further details on the complex structure of the outflow – such as a central jet and localised “bullet” type emission within the high velocity flow – are nicely revealed by the IRAM 30-m CO $J = 2$ –1 maps by Rodríguez-Franco et al. (1999). Within the Odin 126'' antenna beam there is also an N-S extended quiescent molecular cloud structure (the *ridge*), with densities of 10⁴–10⁶ cm⁻³ and temperatures in the range 20–60 K, and characterised by line widths of 3–5 km s⁻¹ and an abrupt velocity shift across the KL nebula from $v_{\text{LSR}} = 8$ km s⁻¹ (in the south) to 10 km s⁻¹ (in the north). The large-scale chemical structure of many important ridge molecules is outlined in Ungerechts et al. (1997).

The interaction between the bipolar high-velocity outflow and the surrounding ridge gas produces shock heating and shock enhanced chemistry, markedly visible in terms of bright H₂ emission, strong high- J CO lines and uniquely strong emission from abundant H₂O (Melnick et al. 2000; Olofsson et al. 2003). Also the roughly orthogonal low-velocity outflow component appears to interact with the ambient gas, creating density,

temperature and column density enhancements in the ridge gas. One such feature is the *compact ridge cloud* ($\Delta v = 3$ km s⁻¹; $v_{\text{LSR}} \approx 8$ km s⁻¹) situated only 10–15'' S of IRc 2, on the northern tip of the 8 km s⁻¹ ridge cloud, where complex oxygen-containing molecules have been observed to be abundant. The hot core itself might also be a result of shock-induced compression. A recent finding along these lines is enhanced [CI] forbidden line (³P₂–³P₁) emission north and south of IRc 2 (in a shell of radius $\approx 20''$, where the outflow encounters ambient gas), and proposed to result from CO dissociation in shocks (Pardo et al. 2005).

Although the major source constituents are commonly discussed in the literature as outlined above, we caution readers that observations yielding higher spatial resolutions (e.g. Blake et al. 1996; Wright et al. 1996; Beuther et al. 2005, all employing aperture synthesis) reveal that the KL core composition is in fact more complex and breaks down into further sub-structures of sizes $\lesssim 10^3$ AU.

We present here the observational results and line identifications. Numerical analyses such as column density and rotation temperature estimates are included in an accompanying paper in this A&A issue (Persson et al. 2007, Paper II hereafter).

2. Observations

The present data-set was obtained in a four-part campaign running over 1.5 years, starting in spring 2004 (Feb.–Apr.), followed by fall 2004 (Aug.–Oct.) and continuing in the same manner in 2005. This division naturally arises from the combination of source coordinates and Odin’s orbital plane (Sun-synchronous low Earth orbit) leading to seasonal visibility constraints for low-declination sources such as the Orion nebula.

The dedicated observing period spanned over ~ 1100 revolutions with a very high success rate due to consistently stable spacecraft performance. Each orbit allows 61 min of astronomical observations, whereas the source line-of-sight is occulted by the Earth and its atmosphere for the remaining 35 min of the orbital period. We employed position switching (PSW) in order to acquire cold sky reference spectra. This was implemented by regularly reorienting the entire spacecraft by $-15'$ in RA with a cycle time of 1 min, carried out by the onboard momentum wheels. The resulting efficiency penalty for slew time was low ($< 20\%$).

The beam size and main beam efficiency of Odin’s 1.1 m offset Gregorian telescope at 557 GHz are 2'1 and 0.9, respectively, as measured in continuum observations of Jupiter assuming a Jovian brightness temperature of 145 K and a disc-like source geometry (Frisk et al. 2003).

The pointing is maintained in real time by the attitude control system, assisted by two star trackers with an angular separation of 40°. It has been empirically established that the reconstructed attitude uncertainty is $\leq 15''$ most of the time.

There are four tunable submm receivers of single-sideband (SSB) type in the radiometer, all of which were employed for these measurements. Image band rejection is achieved using Martin-Puplett filters with cooled termination absorbers and Schottky mixers are used for frequency down-conversion. The channels have centre frequencies of 495, 549, 555, and 572 GHz and the design of the receiver system allows simultaneous use of RX555 and RX572, or RX549 and RX495 (Frisk et al. 2003).

The tuning range of 14 GHz was not fully exploited in all channels although the combined results from the complementary pair RX549 and RX555 cover all their accessible frequency range. System temperatures in the passband centres were around

¹ Poster contributions at Symposium No. 231 of The International Astronomical Union, Asilomar 2005. Abstracts available at <http://asilomar.caltech.edu/>

3000–3500 K with few exceptions as measured by switching between the main beam and a hot load at room temperature. For a given tuning, T_{sys} does not change in time by more than a few percent due to the stable conditions and no interfering atmosphere.

The observing strategy was to tune the receivers in 0.5 GHz steps and observe for 25 orbits. The resulting overlap in between adjacent tunings gives a net on-source integration time of $50 \times 61 \times 0.8/2 \approx 20$ h per channel. This commonly used approach was adopted to reduce potential impacts of artificial spectral patterns/transients or baseline effects which could arise in one tuning but conceivably not in both.

Three spectrometers were used: one acousto-optical spectrometer (AOS) and two hybrid autocorrelators (AC1/2). The former has a bandwidth of 1.1 GHz and a channel spacing of 620 kHz, while the latter two can be used in several modes. In the low resolution mode used here, the bandwidth is 700 MHz with 1 MHz channel spacing. The AOS and the ACs have rather different characteristics and therefore we have used slightly different approaches in building the final spectra, hence the division into two parts of the next section.

3. Data reduction

The data reduction has been performed in two parallel, independent efforts by members of the Odin Team situated at the Onsala Space Observatory and in the University of Calgary. The spectra presented in this paper are the products of the data reduction at Onsala. The very similar Calgary results have been used to verify the quality of the spectra shown here. Although a few differences were found for lines at a level below 0.1 K (or below 4σ in terms of the baseline noise), we are encouraged to believe that the majority of such weak lines are real.

3.1. AOS and data from RX549/RX555

3.1.1. Calibration and averaging

There were essentially three complicating factors that needed special consideration in these data sets.

Frequency correction: by using telluric ozone and water (and occasionally rarer lines during the occultation phase, the capability exists to check the frequency setting to a very high accuracy, as is illustrated in Fig. 1. It was found that there was an offset of 0–5 MHz from the commanded value leaning towards the upper value most of the time. Furthermore, on a few occasions the offset was seen to change instantaneously by 2–3 MHz in mid-observation between two apparently stable offset levels. Thus it was deemed necessary to register telluric frequency references at all times and correct the astronomical spectra accordingly. If no atmospheric lines were present in a particular tuning, overlapping astronomical lines inherent to a different but adjacent tuning with a known frequency correction, were cross-correlated to find the proper correction. This method gave consistently positive results and we now believe that the absolute frequency uncertainty is 1 MHz (≈ 0.5 km s⁻¹) at worst.

Channel dependent RMS: probably owing to the large bandwidth of the AOS, the system temperature profiles had rather steep gradients towards the upper and lower edges, often leading to noise temperatures in these portions twice the mid-spectrum values. When averaging together two adjacent tunings, the low-noise central channels from one tuning will be combined with the high-noise edge channels of the other.

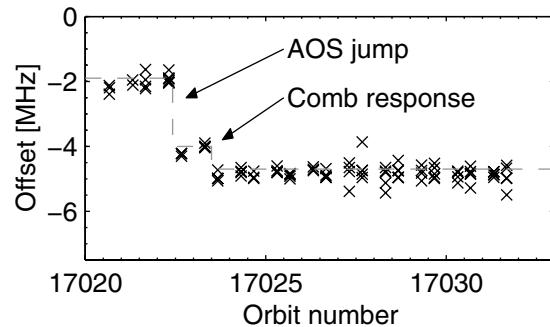


Fig. 1. Tracing the frequency deviation using the telluric H₂¹⁷O line. As is evident, there was an early sudden shift of the line position, corresponding to an AOS laser mode jump during warming up – a small penalty because of our shared astronomy/aeronomy mission. The times of such shifts can be determined accurately since they affect the total power levels of the spectrometer. The gray dashed line shows the correction applied to the data from this sample observation.

This has been taken into account in the weighting procedure by letting the most recently measured T_{sys} profile represent the formal noise *in each channel* of the the next spectrum to be included in the average. Provided that the integration times and resolutions are all the same, and that we have a good linear correlation between T_{sys} and the channel RMS, this approach is easily justified.

Side-band suppression: In general, we have very good suppression of the undesired image band (≥ 20 dB in at least one tuning). In the RX555 tunings, there is one exception where the appearance of an image SO line indicates a suppression of only 10 dB. Similarly poor SSB suppression was seen more frequently in the RX549 data through the emergence of telluric image ozone lines in occultation phase data. As is evident in the final result, we had in general more problems with high T_{sys} and unexplained baseline ripples in this front-end/backend configuration, probably related to the poorer SSB performance. In those cases where image lines were seen in the final average (almost exclusively due to the strong H₂O and ¹³CO lines at 557 and 551 GHz, respectively), the appropriate channels were excluded to remove the interference. The complementary tunings certified that no gaps were created in the total average, although the noise is visibly higher in these portions due to less net observing time. Potential low-level image line intrusions are in general sufficiently weakened not to be seen in our baseline noise, owing to the satellite motion Doppler correction which serves to disperse image band signals.

Other pre-averaging measures consisted of first linearising the readouts of the AOS aided by internal frequency comb measurements, then resampling the AOS spectra to whole MHz to match the AC resolution.

The individual spectra each represent one on-source observation in the PSW cycle which is equivalent to 24 s integration time. During one such observation, the variation of the projected satellite orbital velocity in the direction of the source is not taken into account which introduces a slight spectral smearing of astronomical lines. However, the magnitude of the Doppler shift change *at most* amounts to ~ 200 m s⁻¹ and is considerably less for the major part of the orbit.

The baseline stability was very good (Sect. 3.1.2) and no fits were subtracted from the spectra in the averaging procedure.

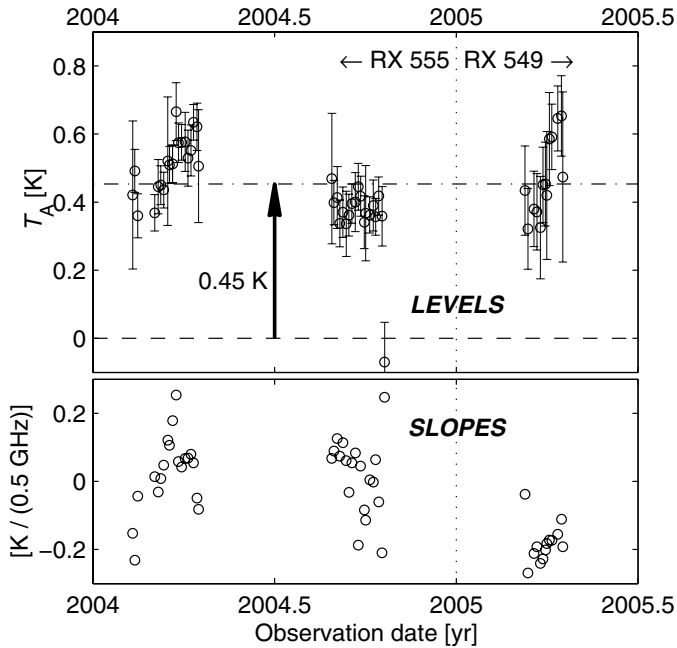


Fig. 2. Baseline levels and slopes in 52 RX555 and RX549 observations before any baseline subtractions. The error bars in the upper panel correspond to 3σ . The slopes are measured as the level difference of two halves of the spectra whose centres are separated by 496 MHz. This figure indeed highlights the stability of the receiver/AOS/calibration chain, but the upwards trends of the levels towards the ends of both spring observing runs remain unexplained. There is also an observation that inexplicably appears to lack continuum signal (while telluric spectral lines could still be detected).

However, to obtain accurate line property estimates for the very weak features, we opted to subtract a piecewise linear fit from the broadband end products, putting the baseline level at zero around clearly detected emission lines.

3.1.2. Baseline stability/continuum level

We have estimated the dust continuum beam averaged antenna temperature around 550 GHz using the spectra from the RX549 and RX555 receivers. One value was extracted for each tuning as shown in Fig. 2 and the average amounted to $T_A = 0.45$ K (1800 Jy beam $^{-1}$).

Due to the crowding of strong lines in some tunings, this calculation relied on noise statistics and did *not* require that the positions of lines were known beforehand. The assumptions made were instead i) at least half the channels in a spectrum were largely unaffected by emission lines, ii) the baselines are largely flat compared to the noise scatter of the intensity in individual spectra, and iii) the noise is Gaussian and the RMS is well described by its formal value derived from the radiometer formula.

The simple procedure was then to sort all channels according to increasing intensity and select the bottom half of the distribution (the top half is “contaminated” by emission lines). Statistically, the expectation value of the distribution is then found by adding $0.8 \times \text{RMS}_{\text{formal}}$ to the mean value of the selected low-intensity channels.

To further remove effects of baseline variations, and to get a handle on the baseline stability, each spectrum was divided into two 500 MHz subspectra on which the calculation described above were performed. The average difference between the two

halves in each tuning then additionally supplied an indication of the first order trend (or slope) of the baselines. Figure 2 also illustrates the results found here. Although it is obvious that a systematic baseline pattern was present throughout the RX549 observations, the RX555 baseline performance is quite satisfactory.

3.2. ACs and data from RX495/RX572

The 700 MHz AC spectra are created by stitching together seven 112 MHz portions. To achieve the double coverage of each frequency interval as we do with the AOS, one AC was split into two portions, 3+4 subbands, and placed on each side of the other AC that covered the central 700 MHz in the passband.

Each such sub-band is typically “well behaved” in terms of having Gaussian noise and a uniform gain curve. However, in the PSW observing mode there is for unknown reasons a linear falloff in channel intensity from the start of each on and off sequence. Due to the inescapable slight asymmetry between on and off measurements, and to the fact that the drift rate changes gradually over the channels in one sub-band, the calibrated spectra end up with a low-level curved saw tooth-like appearance with two sub-bands forming each tooth. This pattern has been removed by using high-order polynomials after careful comparisons with the results obtained by calibrating each sub-band separately. Around the extremely broad CO line at 576.3 GHz, this method failed and the corresponding two tunings were instead cured by employing a corrective procedure that nullifies the effects of the intensity drift mentioned above but is very time-consuming.

The uppermost 200 MHz of the RX495 spectrum were acquired from a tuning that suffered instability; the LO alternated between being properly locked and oscillating between frequency offsets of ± 33 MHz. Using the recorded IF current and the amplitudes of the [CI] forbidden line line at 491.7 GHz (visible in individual spectra, $T_A \approx 6$ K) as guides, about ten minutes of integration was recovered. In spite of the higher noise level thus obtained, we chose to include this spectral section since it contains two strong lines, the [CI] and a low-energy methanol transition ($T_A \approx 1.2$ K).

We did not find any evidence of image band lines interfering in the signal side band for these two receivers, nor did we find any significant frequency offsets (at most ≈ 1 MHz) from nominal values in telluric line position controls in sample tunings.

4. Results

4.1. Summary

Table 1 lists some general figures and characteristics for the survey as a whole. As is evident from this Table, our integrated intensity is dominated by the continuum emission by a ratio of 5:1 (see Sect. 3.1.2 for details). The line-to-continuum ratio found here, 20%, is much lower than that at 350 GHz, 50%, but rather close to the 15% found at 650 GHz (Schilke et al. 2001). For a larger telescope (such as the Herschel Space Observatory) one can expect this value to increase somewhat due to increased intensity from the abundant lines from the compact line sources ($< 10''$) compared to the dust continuum source whose KL component is about $30''$ as seen in for example the 345 GHz bolometer map of Siringo et al. (2004).

Table 1. Survey overview.

Property	Value
Bandwidth covered	42 GHz
Number of lines detected ^a	344
Line density	8 GHz ⁻¹ (range: 4–20)
Line intensity range	0.05–80 K
Number of species detected ^b	38
Typical RMS reached	~25 mK/1 MHz channel
Total $\int T_A dv$	2 455 ^c /2 525 ^d K km s ⁻¹
Total line luminosity ^{e,f}	5×10^{26} W
Mean line-to-continuum ratio ^g	0.2

^a Incl. U- and T-lines (see Sect. 4.4). ^b Including isotopologues and C I. ^c Over all lines detected. ^d Over all measured frequencies. ^e Using the expression $2.65 \times T_r \times \theta / \lambda$ where $\theta = 2.1'$ and λ is given in centimetres, to find the flux density per beam. ^f Using a beam-filling correction factor of 1.25 for data near 490 GHz. ^g Near 550 GHz.

4.2. Spectra and identifications

The final spectral scan results from the four receivers can be seen in Figs. A.1–A.4. The frequency scale is counted w.r.t. a source velocity of $v_{LSR} = +8$ km s⁻¹, and markers are placed at the laboratory rest frequencies of the transitions attributed to the line features.

The general method for identification was to select the most plausible species after comparisons with available molecular databases² (SLAIM03: Lovas 2003; CDMS: Müller et al. 2001; JPL: Pickett et al. 1998) of predicted/calculated or directly measured transition frequencies (SLAIM03 contains both kinds wherever available). The selection criteria included: frequency coincidence, expected abundance, line strength, line width, line velocity, and upper state energy. Where possible we have also used rotation diagram analysis (cf. Goldsmith & Langer 1999) to guide our identification, as discussed in Paper II.

In the case of marginally detected line features suspected to arise from more complex molecules such as dimethyl ether and methyl formate, we also required that other lines of similar expected emission characteristics be visible at other frequencies within the observed bands.

It is important to note that any conceivable artificial sharp features produced in the radiometer would likely be stable in the sky frequency rest frame and thus would be significantly smeared here since the satellite motion Doppler correction of each spectrum varies between -7 and $+7$ km s⁻¹ over one orbit.

The line counts, upper state energy ranges and total integrated intensities for each detected molecule are listed in Table 2. All identifications (molecule and laboratory rest frequency) can be found in Table 6 (available on line).

Also of interest here are the spectral offsets of the measured lines relative to the laboratory frequencies. We have estimated these from the value found at the peak intensity channel of the lines (assuming a systemic emission velocity of $+8$ km s⁻¹) and they are listed in full in Paper II. The average offset per molecule is -0.6 MHz but this cannot be used as a quality measure of the data fidelity nor the accuracy of tabulated rest frequencies since different molecules emit at different velocities (as is likely reflected by the high dispersion, 3.2 MHz). In addition, these emission velocities are often instrument-dependent due to varying beam fillings of the different source components. Nonetheless,

² On line locations at <http://www.cdms.de/> (CDMS) <http://spec.jpl.nasa.gov/> (JPL) (SLAIM03 is not available on line but some of its content is maintained under <http://physics.nist.gov/PhysRefData/>).

Table 2. Summary of all detected species.

Species	Number	Energy range [K]	$\int T_A dv$ [K km s ⁻¹]
CH ₃ OCH ₃	47	106–448	18.3
SO ₂	42	75–737	239.9
³⁴ SO ₂	5	79–457	2.6
SO	5	71–201	181.5
³³ SO	3	191–199	6.5
³⁴ SO	2	191–197	15.6
CH ₃ OH $v_t = 1$	42	332–836	
CH ₃ OH	34	38–863	108.6
¹³ CH ₃ OH	21	37–499	6.8
¹³ CH ₃ OH $v_t = 1$	2	373–670	
CH ₃ CN	17	410–1012	9.3
NO	12	84–232	11.1
CN	8	54	8.5
H ₂ CS	5	138–343	1.7
H ₂ CO	3	106–133	38.5
H ₂ ¹³ CO	1	130	0.6
HD ₂ CO	3	114–141	2.8
OCS	3	604–658	1.3
<i>o</i> -H ₂ O	1	61	320.3
<i>p</i> -H ₂ O	1	867	2.2
<i>o</i> -H ₂ ¹⁷ O	1	61	9.4
<i>o</i> -H ₂ ¹⁸ O	2	60–430	16.2
HD ₂ O	1	66	10.7
HC ₃ N	2	648–799	0.6
CO	1	83	1100
¹³ CO	1	79	174.3
C ¹⁷ O	1	81	6.0
C ¹⁸ O	1	79	24.3
C	1	24	38.7
NH ₃	1	27	20.6
¹⁵ NH ₃	1	27	0.7
HNC	1	91	10.7
N ₂ H ⁺	1	94	1.5
H ₂ S	1	166	4.4
CS	1	129	24
¹³ CS	1	173	v blend
SiO	1	190	17.6
²⁹ SiO	1	187	1.4
³⁰ SiO	1	185	0.5
HCS ⁺	1	186	v blend
NS	1	442	v blend
U-line	28	–	9.1
T-line	36	–	7.2

by choosing the 35 strongest lines of methanol (which conveniently has narrow emission lines), we minimise this effect and get a dispersion of only 1.1 MHz. While this is slightly higher than the stated estimated frequency uncertainty of our spectra, there are a number of possible remaining explanations aside from data error such as lab measurement/calculation error and line blending.

4.3. Important line blends

A means to identify and subsequently remove “interfering” lines is helpful, particularly in the detailed study of line shapes (where the signal-to-noise ratios of the lines are such that this is feasible).

It now seems convincingly clear that the line wings of the rarer isotopologues of water and carbon monoxide are affected by emission from SO₂, ³⁴SO₂, CH₃OH and CH₃CN. Fortunately,

the emission from these species can be accurately modelled due to the wealth of other lines from these species present in our band, allowing determinations of column densities and excitation temperatures. We have in the course of our analysis tried to reconstruct the true shapes of some lines by subtracting polluting emissions from our spectra, and in Paper II one successful example is demonstrated (H_2^{17}O).

We caution that this approach is only useful in contexts where the interfering lines emit in an optically thin portion of the main line (or if the gas is stratified so that the optically thin line arises in the near side of the gas column). For instance, we do not find it likely that the SO_2 line at 556.960 GHz significantly alters the profile of the main water line (at 556.936 GHz) since i) the optical depth towards the centre of the water line is very large, and ii) according to the interpretation in Olofsson et al. (2003) the High Velocity Flow as seen in water is located in front of (or around) the Low Velocity Flow from which the sulphur oxide lines mainly originate, as evidenced by their line widths and source size.

4.4. Unidentified line features

We have defined U-lines – clearly detected lines well distinguished from the baseline noise – and T-lines, which are only marginally visible (T for “Tentative”) against the noise, or in an apparent line blend. The lines of both types are marked in the spectra and listed in Table 3.

We have in some cases found candidate species (Table 3) which have not fulfilled all our criteria for an unequivocal designation and they are kept as U- or T-lines. Some of the more interesting scenarios are discussed below.

4.4.1. New SO^+ lines?

Interstellar SO^+ was first detected in the shocked clump IC443G, presumably being formed in the dissociative shock caused by the supernova remnant (Turner 1992). Our weak unidentified lines at 486.845 and 487.209 GHz tentatively can be identified as the $J = 21/2-19/2$ e and f doublet of the reactive radical SO^+ in its $^2\Pi_{1/2}$ ground state (JPL; Amano et al. 1991). The suggested assignment is consistent with the detection in Orion KL of lower energy SO^+ lines at 115.804, 116.180, 208.590, and 255.353 GHz (Turner 1994). Our assignment is further strengthened by the U-line at 347.743 GHz observed by Schilke et al. (1997) which we identify here with the $J = 15/2-13/2$ e transition of SO^+ at 347.740 GHz. However, the corresponding f transition at 348.115 GHz is hidden in a blend with $^{13}\text{CH}_3\text{OH}$ and $^{34}\text{SO}_2$.

4.4.2. Other notable frequency coincidences: SH^- and ND

Our weak, slightly broad lines near 546.138 and 546.176 GHz could be associated with the $N_J = 1_1-0_1$ hyperfine transition cluster of the ND radical in its $X^3\Sigma^-$ ground vibronic state (CDMS; Saito & Goto 1993; Takano et al. 1998). If so, the strongest component is at a blue-shifted position closer to the Hot Core velocity, in agreement to what is seen in other nitrogen hydrides such as NH_2 (which we tentatively conclude to be blue-shifted after studying the 900 GHz spectral survey of Comito et al. 2005 in detail). NH_3 on the other hand – discussed further in Paper II – has a $\sim 60\%$ Hot Core contribution but this is heavily masked by its optical depth in both the Hot Core and in the

Table 3. Unidentified (U) and/or marginally detected (T) lines.

Frequency [MHz]	Type [U/T]	Sugg. ident.	Table <i>continued</i>	
486 845	T	SO^+	555 914	T –
487 209	U	SO^+	555 933	T –
487 507	T	CH_3CHO	556 267	T –
488 477	T	–	556 633	T –
488 598	U	CH_3OCHO	559 239	U CH_3OCHO
488 633	U	CH_3CHO	559 816	T HDO
489 193	T	–	559 861	U CH_3OCHO
489 709	T	SiS	559 913	U –
491 496	U	CH_3OCHO	560 753	T –
491 892	U	–	561 971	U –
541 926	T	–	562 118	T –
541 981	U	CH_3OCHO	562 960	U –
542 945	U	–	563 033	U –
543 873	U	–	563 481	T HNCO
544 016	T	SiS	564 105	U –
546 138	U	ND	564 418	T SH^-
546 176	T	ND	566 066	U –
546 662	T	–	567 485	U –
546 805	T	–	569 138	U HNCO
547 080	T	–	570 303	U –
547 162	T	–	570 335	T –
547 262	T	HNCO	570 790	T –
549 142	T	HNCO	570 814	T –
549 199	T	$\text{HNCO}, \text{H}_2\text{CS}$	571 151	T HNCO
549 449	U	–	571 217	T HNCO
549 719	T	$\text{SO}_2, (\text{CH}_3)_2\text{O}$	571 477	T $\text{H}_2\text{C}^{18}\text{O}$
550 132	T	SO_2	572 596	U –
552 308	U	–	572 678	U –
552 846	T	–	574 184	U –
553 667	U	CH_3OCHO	575 397	T –
553 716	U	–	576 446	U –
555 312	T	–	577 160	T –

Compact Ridge. Unfortunately, the predicted shape of the line bundle as a whole does not match the observation and one would need to invoke non-LTE excitation to explain this difference.

A weak unidentified line at 564.418 GHz may originate in the $J = 1-0$ rotational transition of SH^- in its $X^1\Sigma^+$ ground state, measured to fall at the frequency 564.422 GHz (Civiš et al. 1998). A new interstellar anion would be of utmost interest since only one has been found previously, namely the discovery of C_6H^- which was recently reported by McCarthy et al. (2006). Thus – although our line is not strong enough to claim a detection ($\sim 3.5\sigma$ relative to the local noise) – we chose to perform a very simple column density calculation (or an upper limit thereof if the line turned out false). By employing the LTE assumption with full beamfilling, an excitation temperature of 100 K, and a dipole moment of 0.273 D (adopted from the ab initio calculations of Senekowitsch et al. 1985), we arrive at a figure of $N_{\text{SH}^-} = 2 \times 10^{13} \text{ cm}^{-2}$. The scenario used would be consistent with SH^- residing in the extended OMC-1/M42 face-on PDR (discussed in Wirström et al. 2006). Should the origin of the line (if real) be any of the smaller Orion KL components – as indeed the observed line width ($\Delta v_{\text{FWHM}} = 11 \text{ km s}^{-1}$) seems to indicate – the column density rises by a factor of ~ 200 . We deem at least the PDR column density to be a reasonably low value in light of the rather unknown chemistry of similar hydrides in

the interstellar medium. The SH radical, for instance, has only been found in the atmosphere of a Mira variable through mid-IR transitions (Yamamura et al. 2000). Nevertheless, a possible contribution from SH in a C₃ spectrum towards Sgr B2 has been reported by Cernicharo et al. (2000). We also note that a formation pathway exists involving H₂S (via dissociative electron attachment), a molecule observed by Odin in the present survey and treated in Paper II.

Both these candidates (marked by gray arrows in the spectra figures) can be confirmed or ruled out by the forthcoming Herschel mission (discussed further in Sect. 5). For the case of ND, the triplets of NH at 947 and 1000 GHz are also relevant.

4.5. Non-detections

Two notable non-detections have been indicated by gray arrows in our spectra: the PH and O₂ molecules. The PH line (a hyperfine transition within the $N_J = 1_1-0_1$ group at 553.363 GHz) has also been searched for in IRC + 10216 by Odin to a much higher sensitivity by Bernath et al. (2007), and we refer to them for details on the PH physical and chemical properties and its role in the circum- and interstellar medium. The O₂ line at 487.249 GHz has previously been searched for by the SWAS satellite (having a larger beam size) down to a sensitivity of 6.4 mK (Goldsmith et al. 2000) without success. Both O₂ non-detections are consistent with the Odin upper limit from the ground state transition at 118.750 GHz by Pagani et al. (2003).

4.6. Improvements of existing spectroscopic data

In the case of our rather weak H₂CS lines, we did at first find frequency offsets between 6 and 14 MHz systematically redwards of the expected values (as given in the JPL database which indeed stated high uncertainties for these calculated H₂CS frequencies). Prompted by private communication, an entry for this molecule was subsequently inserted into CDMS and the new calculated rest frequencies found there gave very good agreements with our measured positions in all but one line. This is an encouraging result proving that large measured frequency offsets are likely not to be spurious and may in some cases indicate that the existing tabulated spectroscopy data are off the mark.

In the case of H₂CS, new extensive laboratory spectroscopy work has kindly been performed by Eric Herbst and his collaborators. The resulting H₂CS database will be crucial for Herschel Space Observatory.

In general, we hope that our measured line parameters (listed in bulk in Paper II) may be useful for accurate determination of molecular data such as rotational constants.

5. Discussion of future observations

No further Odin observations of this kind are currently planned and the observation time cost for significant noise reduction would in any case be prohibitive. However, the spectral portions presented here will be reobserved by the Herschel space observatory³ and is of interest to briefly discuss what they could obtain. Herschel is a European Space Agency (ESA) satellite mission aimed at launching a 3.5 m telescope equipped with very low noise submm/far-IR heterodyne receivers in 2008.

Most of the identified lines in this survey belong to species already observed at other transitions (at both lower and higher

frequencies) and source size estimates for the corresponding emission components are available in the literature (e.g. references in Sect. 1 and Paper II). A rough Herschel beam-filling estimate based on these source sizes reveals that those lines will be 1–10 times stronger in the Herschel spectrum, with the majority leaning towards the higher end. Assuming further an observation time of only one hour in combination with recent figures for the Herschel receiver system sensitivity, one finds that the signal-to-noise ratio will be increased by up to a factor of 20 in such a case. This will be particularly useful for the weakest lines (5–10 σ) seen in the Odin survey which will be possible to study in some detail in the Herschel spectrum. It is in this group we find nearly all the unidentified lines and the potential for new discoveries among them is obvious. The interesting frequency coincidences of SH⁻ and ND described earlier are good examples. The interpretation of these and even weaker lines runs, however, the risk of being hampered by line crowding and blending (already up to 20 lines/GHz in our spectrum) due to the plethora of lines that will emerge from the noise compared to the Odin spectrum. This in turn will put high demands on the system baseline stability in order to correctly disentangle the emissions. The pollutive contributions in the key water isotopologue lines discussed above will also be worsened (due to differential beam-fillings) and on a side note one can predict that this problem will arise in most sources where Herschel observes these species.

6. Conclusions

We have conducted a spectral survey in two submillimetre windows largely inaccessible from the ground due to atmospheric opacity. The frequency ranges covered are: 486.4–492.3 and 541.5–577.6 GHz. This was achieved using the Odin submm satellite.

The spacecraft performance was generally excellent in terms of high observing efficiency and good sideband suppression most of the time (within the SSB receivers).

The baseline stability has been shown to be satisfactory, albeit high-order polynomials being required in about 50% of the data to remove a fixed pattern arising in the autocorrelators in this particular observation setup.

Careful attention has been paid to the frequency alignment of our data resulting in an estimated frequency error of ≤ 1 MHz.

Thus, high confidence is warranted in the fidelity of the reduced spectra. To ascertain the calibration accuracy, some lines have also been compared to previous or later targeted Odin observations using markedly different instrumental setups.

We found a total of 280 identified emission lines (some of which include multiple transitions), and 28 unidentified lines. We have also pointed out a further 36 borderline detected features which in some cases have interesting candidate assignments such as SH⁻ and SO⁺.

Among the 38 detected molecules, we have four water isotopologues seen in at least five emission lines. These data are used in Paper II to make a water abundance analysis.

Column density estimates for all species are presented in Paper II, as well as abundance, source size, and rotation temperature estimates for a selection of molecules.

Acknowledgements. Generous financial support from the Research Councils and Space Agencies in Sweden, Canada, Finland and France is gratefully acknowledged. We sincerely thank Frank Lovas for a CD containing his molecular spectroscopy database SLAIM03, and the dedicated scientists at Cologne (CDMS) and at JPL for undertaking the all-important work of providing spectroscopic data through the internet.

³ <http://www.esa.int/science/herschel>

References

- Amano, T., Amanao, T., & Warner, H. E. 1991, *J. Mol. Spectrosc.*, 146, 519
- Bernath, P., Kwok, S., Koning, N., et al. 2007, *ApJ*, submitted
- Beuther, H., Zhang, Q., Greenhill, L. J., et al. 2005, *ApJ*, 632, 355
- Beuther, H., Zang, Q., Reid, M. J., et al. 2006, *ApJ*, 636, 323
- Blake, G. A., Mundy, L. G., Carlstrom, J. E., et al. 1996, *ApJ*, 472, L49
- Cernicharo, J., Goicoechea, J. R., & Caux, E. 2000, *ApJ*, 534, L199
- Civiš, S., Walters, A., Yu Tretyakov, M., Bailleux, S., & Bogey, M. 1998, *J. Chem. Phys.*, 108, 8369
- Comito, C., Schilke, P., Phillips, T. G., et al. 2005, *ApJS*, 156, 127
- Frisk, U., Hagström, M., Ala-Laurinaho, J., et al. 2003, *A&A*, 402, L27
- Genzel, R., & Stutzki, J. 1989, *ARA&A*, 27, 41
- Goldsmith, P. F., & Langer, W. D. 1999, *ApJ*, 517, 209
- Goldsmith, P. F., Melnick, G. J., Bergin, E. A., et al. 2000, *ApJ*, 539, L123
- de Graauw, Th., & Helmich, F. P. 2000, in *Proc. Symp., The Promise of the Herschel Space Observatory*, ed. G. L. Pilbratt, J. Cernicharo, A. M. Heras, T. Prusti, & R. Harris, 45
- Johansson, L. E. B., Andersson, C., Elldér, et al. 1984, *A&A*, 130, 227
- Johansson, L. E. B., Andersson, C., Elldér, et al. 1985, *A&AS*, 60, 135
- Lee, C. W., & Cho, S.-H. 2002, *JKAS*, 35, 187
- Lovas, F. J. 2003, *Spectral Line Atlas for Interstellar Molecules (SLAIM) Ver. 1*, private communication
- McCarthy, M. C., Gottlieb, C. A., Gupta, H., & Thaddeus, P. 2006, *ApJ*, 652, L141
- Melnick, G. J., Ashby, M. L. N., Plume, R., et al. 2000, *ApJ*, 539, L87
- Müller, H. S. P., Thorwirth, S., Roth, D. A., & Winnewisser, G. 2001, *A&A*, 370, L49
- Olofsson, H., Elldér, J., Hjalmarson, Å., & Rydbeck, G. 1982, *A&A*, 113, L18
- Olofsson, A. O. H., Olofsson, G., Hjalmarson, Å., et al. 2003, *A&A*, 402, L47
- Pagani, L., Olofsson, A. O. H., Bergman, P., et al. 2003, *A&A*, 402, L77
- Pardo, R. P., Cernicharo, J., Herpin, F., et al. 2001, *ApJ*, 562, 799
- Pardo, J. R., Cernicharo, J., & Phillips, T. G. 2005, *ApJ*, 634, L61
- Persson, C. M., Olofsson, A. O. H., Koning, N., et al. 2007, *A&A*, 476, 807 (Paper II)
- Pickett, H. M., Poynter, R. L., Cohen, E. A., et al. 1998, *J. Quant. Spectrosc. & Rad. Trans.*, 60, 883
- Rodríguez-Franco, A., Martín-Pintado, J., & Wilson, T. L. 1999, *A&A*, 344, L57
- Schilke, P., Groesbeck, T. D., Blake, G. A., & Phillips, T. G. 1997, *ApJS*, 108, 301
- Saito, S., & Goto, M. 1993, *ApJ*, 410, L53
- Schilke, P., Benford, D. J., Hunter, T. R., Lis, D. C., & Phillips, T. G. 2001, *ApJS*, 132, 281
- Sempere, M. J., Cernicharo, J., Leflouch, B., & González-Alfonso, E. 2000, *ApJ*, 530, L123
- Senekowitsch, J., Werner, H.-J., Rosmus, P., Reinsch, E.-A., & O'Neil, S. V. 1985, *J. Chem. Phys.*, 83, 4661
- Siringo, G., Kreysa, E., Reichertz, L. A., & Menten, K. M. 2004, *A&A*, 422, 751
- Takano, S., Klaus, T., & Winnewisser, G. 1998, *J. Mol. Spectrosc.*, 192, 309
- Turner, B. E. 1992a, *ApJ*, 396, L107
- Turner, B. E. 1992b, *ApJ*, 430, 727
- Ungerechts, H., Bergin, E. A., Goldsmith, P. F., et al. 1997, *ApJ*, 482, 245
- White, G. J., Araki, M., Greaves, J. S., Ohishi, M., & Higginbottom, N. S. 2003, *A&A*, 407, 589
- Wirström, E. S., Bergman, P., Olofsson, A. O. H., et al. 2006, *A&A*, 453, 979
- Wright, M. C. H., Plambeck, R. L., & Wilner, D. J. 1996, *ApJ*, 469, 216
- Yamamura, I., Kawaguchi, K., & Ridgway, S. T. 2000, *ApJ*, 528, L33
- Zuckerman, B., & Palmer, P. 1975, *ApJ*, 199, L35

Appendix A: Spectra

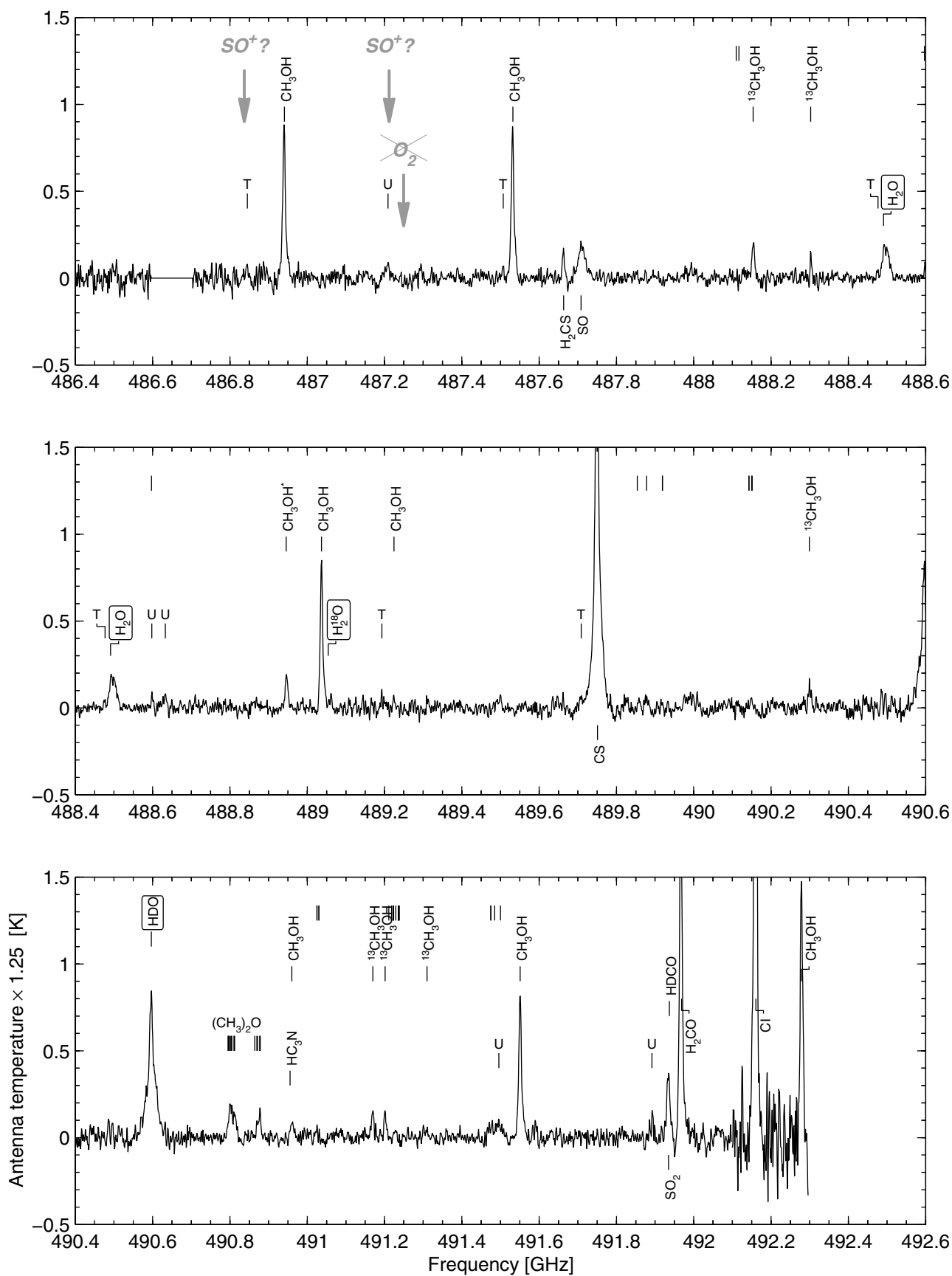


Fig. A.1. The Odin spectral survey between 486.4 and 492.1 GHz (RX495). Note the intensity scaling factor of 1.25 to approximately deconvolve the spectrum to the beam size near 557 GHz (assuming a point source). Empty markers at the intensity level of 1.25 K denote CH_3OCHO lines.

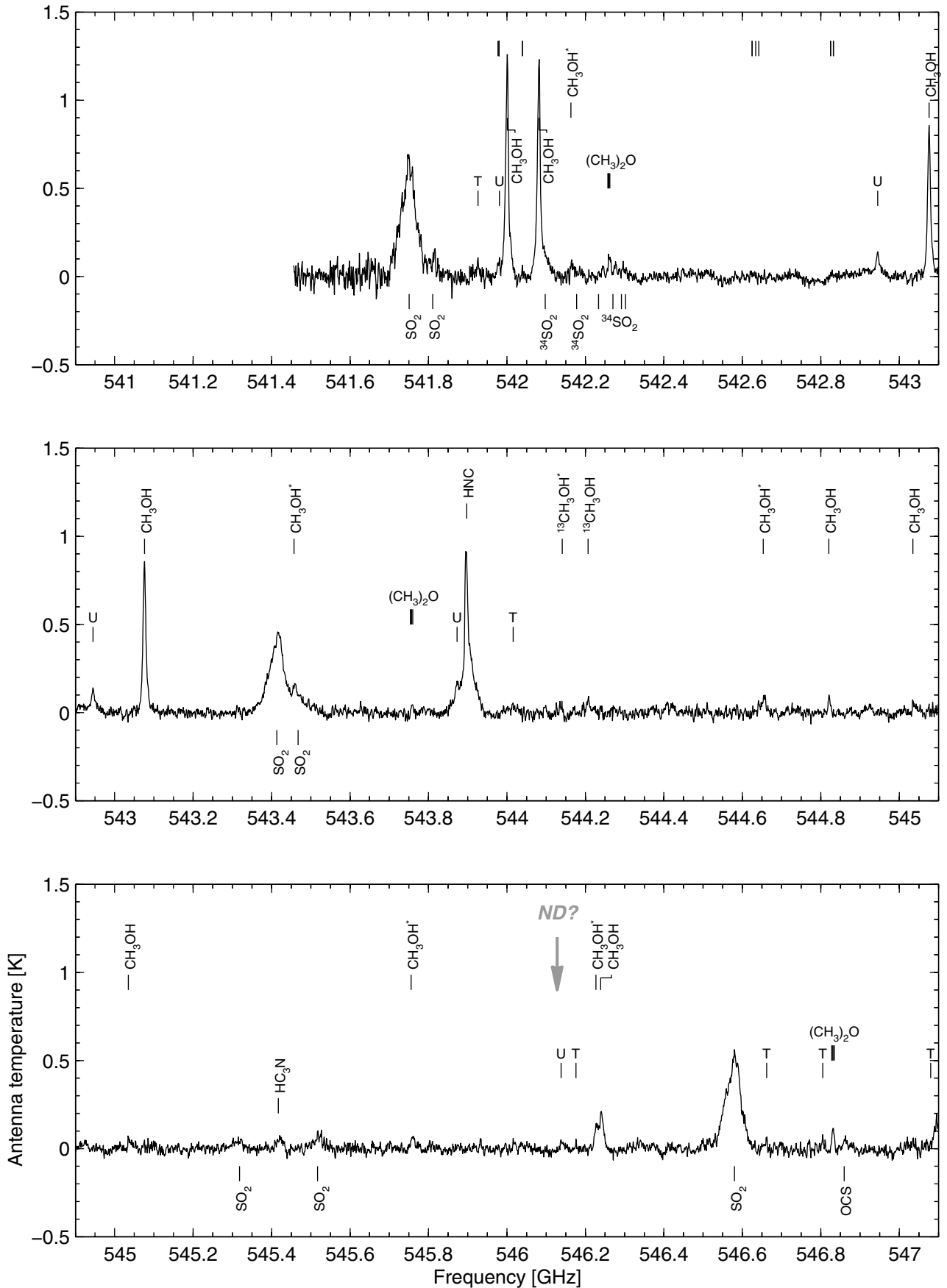


Fig. A.2. The Odin spectral survey between 541.4 and 547.1 GHz (RX549). Empty markers at the intensity level of 1.25 K denote CH_3OCHO lines. A star denotes a transition within a vibrationally excited state: $\nu_1 = 1$ for methanol, and $\nu_2 = 1$ for SO_2 .

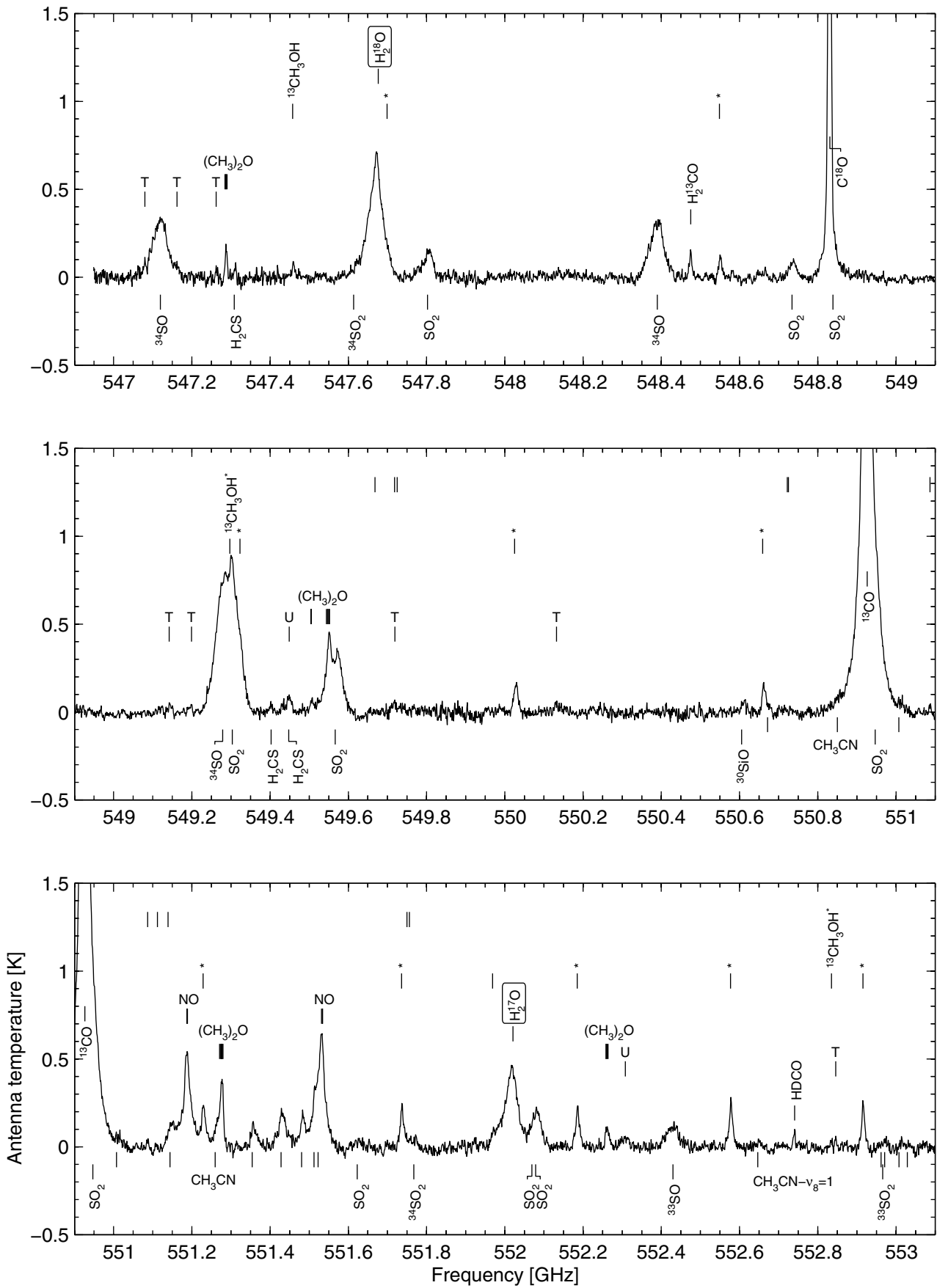


Fig. A.3. The Odin spectral survey between 546.9 and 563.1 GHz (RX555). Unlabelled markers at intensity levels -0.1 , 0.5 , 0.9 , and 1.25 K, belong to SO_2 , $(\text{CH}_3)_2\text{OH}$, CH_3OH , and CH_3OCHO , respectively. A star denotes a transition within a vibrationally excited state: $v_t = 1$ for methanol, and $v_2 = 1$ for SO_2 . Two sets of markers immediately below the spectrum baseline belong to ground state and vibrationally excited CH_3CN .

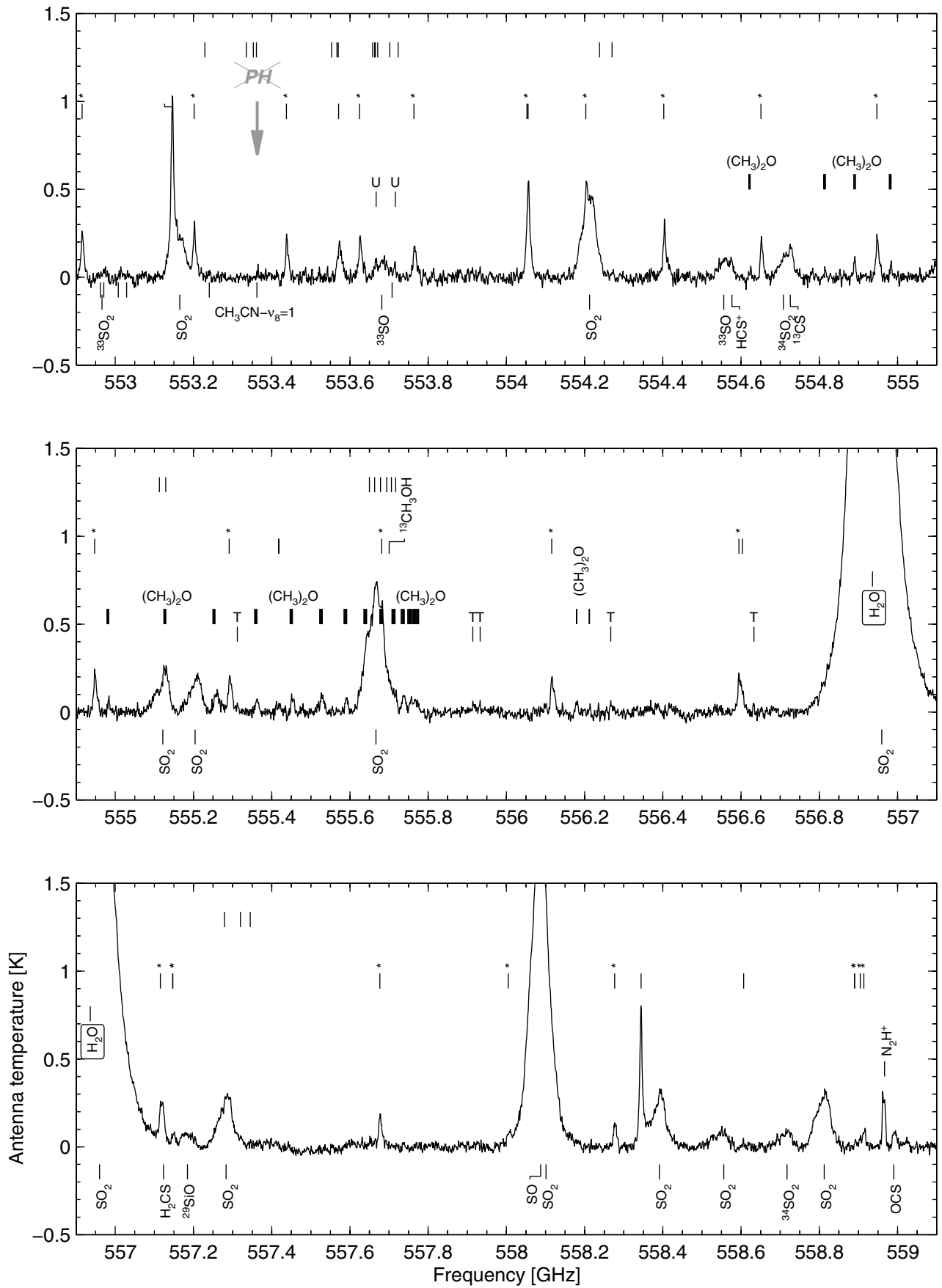


Fig. A.3. continued.

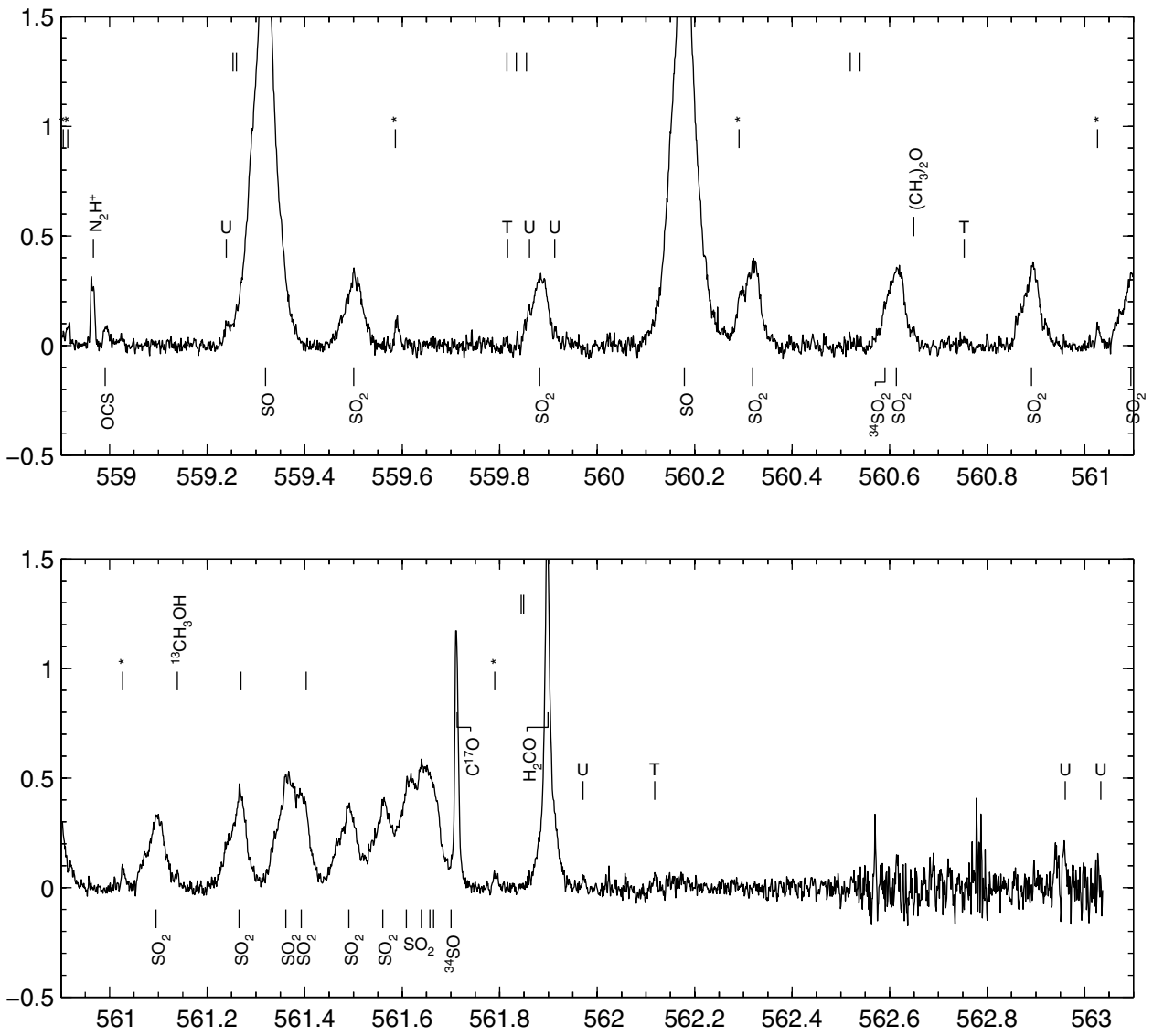


Fig. A.3. continued.

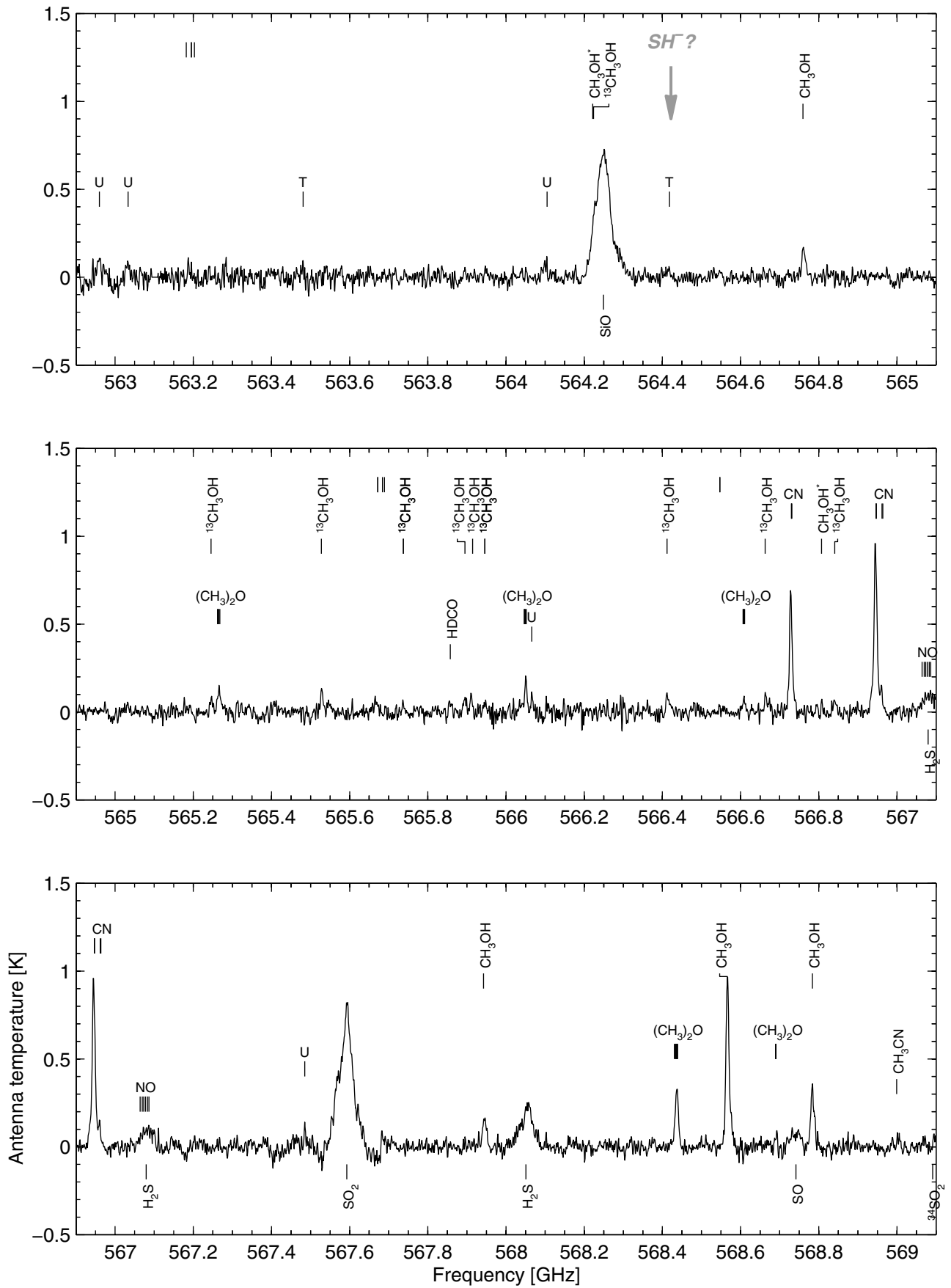


Fig. A.4. The Odin spectral survey between 562.9 and 577.6 GHz (RX572). Empty markers at the intensity level of 1.25 K denote CH_3OCHO lines.

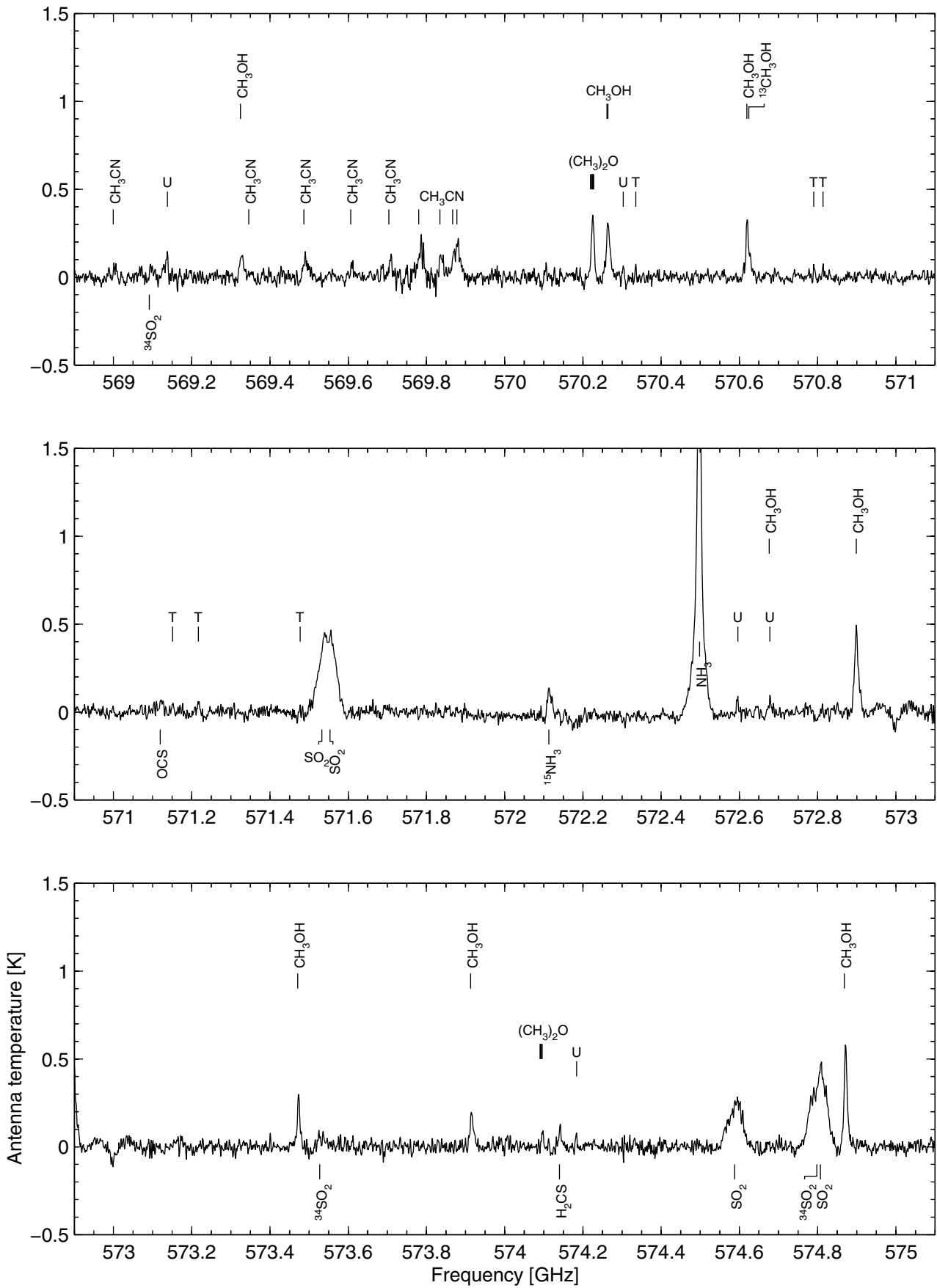


Fig. A.4. continued.

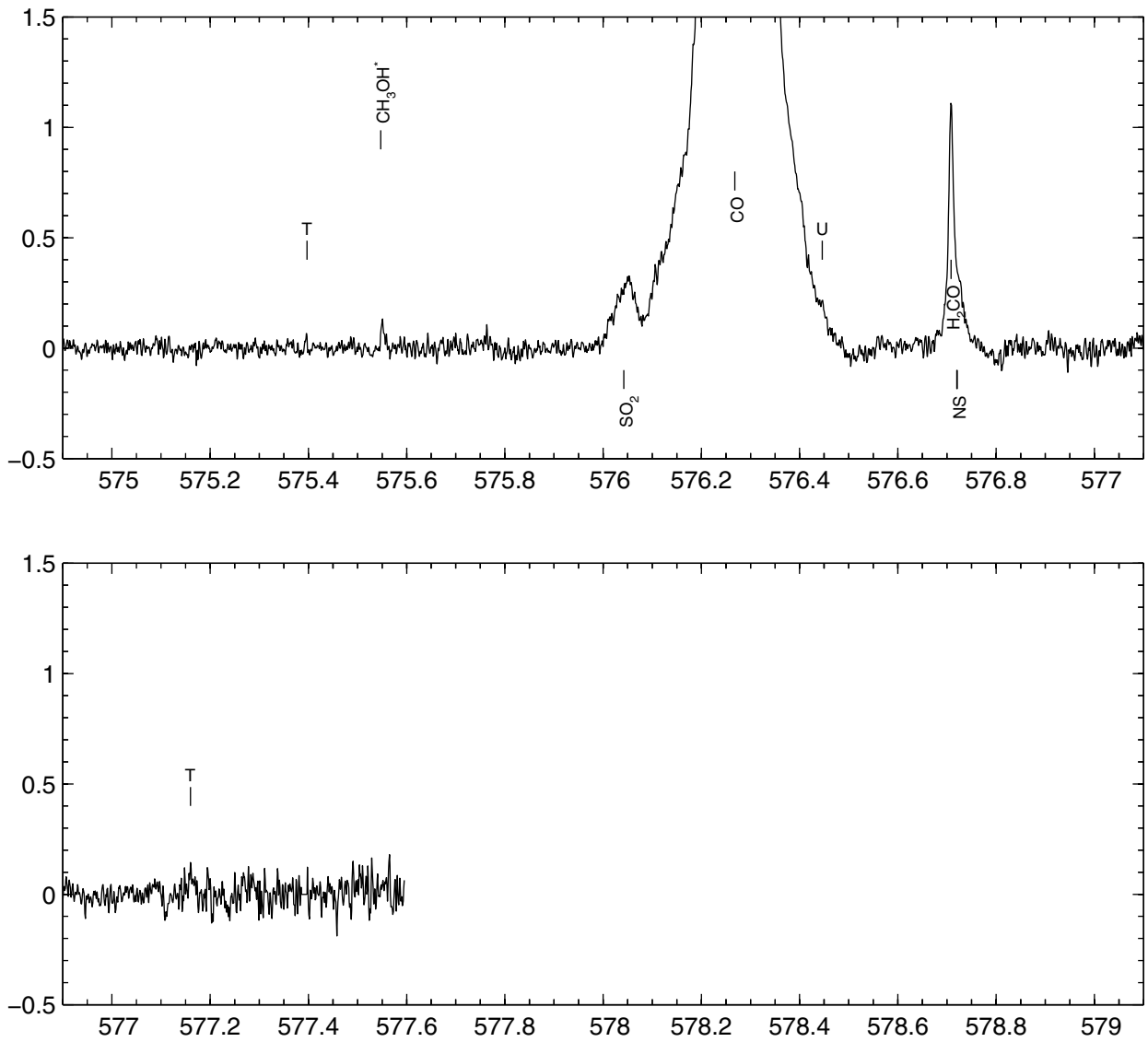


Fig. A.4. continued.

Online Material

Appendix B: Electronic table on lines**Table B.1.** Lines detected towards Orion KL listed in order of laboratory frequency.

Frequency [MHz]	Molecule or U/T-line	Frequency [MHz]	Molecule or U/T-line	Frequency [MHz]	Molecule or U/T-line
486 845	T-line	541 926	T-line	547 286.2	CH ₃ OCH ₃
486 940.9	CH ₃ OH	541 981	U-line	547 287.8	CH ₃ OCH ₃
487 209	U-line	542 000.9	CH ₃ OH	547 290.1	CH ₃ OCH ₃
487 507	T-line	542 081.9	CH ₃ OH	547 308.2	H ₂ CS
487 531.9	CH ₃ OH	542 097.7	³⁴ SO ₂	547 457.8	¹³ CH ₃ OH
487 663.4	H ₂ CS	542 163.0	CH ₃ OH	547 613.5	³⁴ SO ₂
487 708.5	SO	542 177.4	³⁴ SO ₂	547 676.4	<i>ortho</i> -H ₂ ¹⁸ O
488 153.5	¹³ CH ₃ OH	542 233.5	³⁴ SO ₂	547 698.9	CH ₃ OH
488 302.6	¹³ CH ₃ OH	542 257.7	CH ₃ OCH ₃	547 802.2	SO ₂
488 477	T-line	542 257.7	CH ₃ OCH ₃	548 389.8	³⁴ SO
488 491.1	<i>para</i> -H ₂ O	542 260.1	CH ₃ OCH ₃	548 475.2	H ¹³ CO
488 598	U-line	542 262.4	CH ₃ OCH ₃	548 548.7	CH ₃ OH
488 633	U-line	542 270.1	³⁴ SO ₂	548 734.3	SO ₂
488 945.5	CH ₃ OH	542 291.7	³⁴ SO ₂	548 831.0	C ¹⁸ O
489 037.0	CH ₃ OH	542 302.3	³⁴ SO ₂	548 838.9	SO ₂
489 054.3	<i>ortho</i> -H ₂ ¹⁸ O	542 945	U-line	549 142	T-line
489 193	T-line	543 076.1	CH ₃ OH	549 199	T-line
489 224.3	CH ₃ OH	543 413.5	SO ₂	549 278.7	³⁴ SO
489 709	T-line	543 457.3	CH ₃ OH	549 297.1	¹³ CH ₃ OH
489 751.1	CS	543 467.7	SO ₂	549 303.3	SO ₂
490 299.4	¹³ CH ₃ OH	543 753.9	CH ₃ OCH ₃	549 322.8	CH ₃ OH
490 596.7	HDO	543 753.9	CH ₃ OCH ₃	549 402.4	H ₂ CS
490 795.3	CH ₃ OCH ₃	543 756.9	CH ₃ OCH ₃	549 447.5	H ₂ CS
490 795.3	CH ₃ OCH ₃	543 759.8	CH ₃ OCH ₃	549 449	U-line
490 797.5	CH ₃ OCH ₃	543 873	U-line	549 504.7	CH ₃ OCH ₃
490 798.3	CH ₃ OCH ₃	543 897.6	HNC	549 504.7	CH ₃ OCH ₃
490 801.3	CH ₃ OCH ₃	544 016	T-line	549 504.9	CH ₃ OCH ₃
490 804.3	CH ₃ OCH ₃	544 140.5	¹³ CH ₃ OH	549 505.2	CH ₃ OCH ₃
490 804.7	CH ₃ OCH ₃	544 206.7	¹³ CH ₃ OH	549 543.8	CH ₃ OCH ₃
490 810.3	CH ₃ OCH ₃	544 653.1	CH ₃ OH	549 546.5	CH ₃ OCH ₃
490 811.4	CH ₃ OCH ₃	544 820.5	CH ₃ OH	549 547.4	CH ₃ OCH ₃
490 812.1	CH ₃ OCH ₃	545 034.8	CH ₃ OH	549 547.7	CH ₃ OCH ₃
490 864.4	CH ₃ OCH ₃	545 318.5	SO ₂	549 550.4	CH ₃ OCH ₃
490 869.8	CH ₃ OCH ₃	545 417.1	HC ₃ N	549 550.6	CH ₃ OCH ₃
490 871.5	CH ₃ OCH ₃	545 517.3	SO ₂	549 550.8	CH ₃ OCH ₃
490 877.2	CH ₃ OCH ₃	545 755.6	CH ₃ OH	549 551.7	CH ₃ OCH ₃
490 877.6	CH ₃ OCH ₃	546 138	U-line	549 566.4	SO ₂
490 878.3	CH ₃ OCH ₃	546 176	T-line	549 719	T-line
490 955.7	HC ₃ N	546 226.8	CH ₃ OH	550 025.2	CH ₃ OH
490 960.0	CH ₃ OH	546 239.0	CH ₃ OH	550 132	T-line
491 170.0	¹³ CH ₃ OH	546 579.8	SO ₂	550 605.2	³⁰ SiO
491 201.3	¹³ CH ₃ OH	546 662	T-line	550 659.3	CH ₃ OH
491 310.1	¹³ CH ₃ OH	546 805	T-line	550 671.7	CH ₃ CN
491 496	U-line	546 827.8	CH ₃ OCH ₃	550 850.0	CH ₃ CN
491 550.9	CH ₃ OH	546 829.2	CH ₃ OCH ₃	550 926.3	¹³ CO
491 892	U-line	546 831.5	CH ₃ OCH ₃	550 946.7	SO ₂
491 934.7	SO ₂	546 834.5	CH ₃ OCH ₃	551 007.4	CH ₃ CN
491 937.0	HDCO	546 859.8	OCS	551 143.9	CH ₃ CN
491 968.4	H ₂ CO	547 080	T-line	551 187.3	NO
492 160.7	C	547 119.6	³⁴ SO	551 187.5	NO
492 278.7	CH ₃ OH	547 162	T-line	551 188.8	NO
541 750.9	SO ₂	547 262	T-line	551 228.6	CH ₃ OH
541 810.6	SO ₂	547 284.8	CH ₃ OCH ₃	551 259.6	CH ₃ CN

Table B.1. continued.

Frequency [MHz]	Molecule or U/T-line	Frequency [MHz]	Molecule or U/T-line	Frequency [MHz]	Molecule or U/T-line
551 270.8	CH ₃ OCH ₃	554 055.5	CH ₃ OH	555 253.8	CH ₃ OCH ₃
551 273.6	CH ₃ OCH ₃	554 202.9	CH ₃ OH	555 253.8	CH ₃ OCH ₃
551 275.1	CH ₃ OCH ₃	554 212.8	SO ₂	555 254.9	CH ₃ OCH ₃
551 275.1	CH ₃ OCH ₃	554 402.5	CH ₃ OH	555 291.1	CH ₃ OH
551 276.5	CH ₃ OCH ₃	554 555.6	³³ SO	555 312	T-line
551 276.5	CH ₃ OCH ₃	554 576.6	HCS ⁺	555 356.8	CH ₃ OCH ₃
551 277.9	CH ₃ OCH ₃	554 619.8	CH ₃ OCH ₃	555 356.8	CH ₃ OCH ₃
551 279.4	CH ₃ OCH ₃	554 619.8	CH ₃ OCH ₃	555 358.3	CH ₃ OCH ₃
551 354.2	CH ₃ CN	554 621.0	CH ₃ OCH ₃	555 359.5	CH ₃ OCH ₃
551 427.9	CH ₃ CN	554 621.5	CH ₃ OCH ₃	555 359.9	CH ₃ OCH ₃
551 480.6	CH ₃ CN	554 622.1	CH ₃ OCH ₃	555 361.1	CH ₃ OCH ₃
551 512.2	CH ₃ CN	554 622.6	CH ₃ OCH ₃	555 361.1	CH ₃ OCH ₃
551 522.7	CH ₃ CN	554 622.6	CH ₃ OCH ₃	555 362.3	CH ₃ OCH ₃
551 531.5	NO	554 623.2	CH ₃ OCH ₃	555 417.7	CH ₃ OH
551 534.0	NO	554 650.9	CH ₃ OH	555 418.5	CH ₃ OH
551 534.1	NO	554 708.2	³⁴ SO ₂	555 447.3	CH ₃ OCH ₃
551 622.9	SO ₂	554 726.0	¹³ CS	555 447.3	CH ₃ OCH ₃
551 736.2	CH ₃ OH	554 811.5	CH ₃ OCH ₃	555 448.9	CH ₃ OCH ₃
551 767.4	³⁴ SO ₂	554 811.5	CH ₃ OCH ₃	555 450.2	CH ₃ OCH ₃
551 968.8	CH ₃ OH	554 812.7	CH ₃ OCH ₃	555 450.6	CH ₃ OCH ₃
552 021.0	<i>ortho</i> -H ₂ ¹⁷ O	554 813.4	CH ₃ OCH ₃	555 451.9	CH ₃ OCH ₃
552 069.4	SO ₂	554 813.9	CH ₃ OCH ₃	555 451.9	CH ₃ OCH ₃
552 078.9	SO ₂	554 814.6	CH ₃ OCH ₃	555 453.1	CH ₃ OCH ₃
552 184.8	CH ₃ OH	554 814.6	CH ₃ OCH ₃	555 522.9	CH ₃ OCH ₃
552 258.9	CH ₃ OCH ₃	554 815.3	CH ₃ OCH ₃	555 522.9	CH ₃ OCH ₃
552 258.9	CH ₃ OCH ₃	554 888.3	CH ₃ OCH ₃	555 524.6	CH ₃ OCH ₃
552 261.4	CH ₃ OCH ₃	554 888.3	CH ₃ OCH ₃	555 526.0	CH ₃ OCH ₃
552 264.0	CH ₃ OCH ₃	554 890.4	CH ₃ OCH ₃	555 526.4	CH ₃ OCH ₃
552 308	U-line	554 892.5	CH ₃ OCH ₃	555 527.8	CH ₃ OCH ₃
552 429.8	³³ SO	554 947.4	CH ₃ OH	555 527.8	CH ₃ OCH ₃
552 577.2	CH ₃ OH	554 979.1	CH ₃ OCH ₃	555 529.2	CH ₃ OCH ₃
552 646.6	CH ₃ CN	554 979.1	CH ₃ OCH ₃	555 585.3	CH ₃ OCH ₃
552 740.9	HDCO	554 980.4	CH ₃ OCH ₃	555 585.3	CH ₃ OCH ₃
552 835.1	¹³ CH ₃ OH	554 981.2	CH ₃ OCH ₃	555 587.1	CH ₃ OCH ₃
552 846	T-line	554 981.7	CH ₃ OCH ₃	555 588.6	CH ₃ OCH ₃
552 915.4	CH ₃ OH	554 982.5	CH ₃ OCH ₃	555 589.0	CH ₃ OCH ₃
552 970.8	CH ₃ CN	554 982.5	CH ₃ OCH ₃	555 590.4	CH ₃ OCH ₃
553 007.8	CH ₃ CN	554 983.3	CH ₃ OCH ₃	555 590.4	CH ₃ OCH ₃
553 029.1	CH ₃ CN	555 121.5	SO ₂	555 591.9	CH ₃ OCH ₃
553 146.3	CH ₃ OH	555 124.5	CH ₃ OCH ₃	555 635.9	CH ₃ OCH ₃
553 164.9	SO ₂	555 124.5	CH ₃ OCH ₃	555 635.9	CH ₃ OCH ₃
553 201.6	CH ₃ OH	555 125.9	CH ₃ OCH ₃	555 637.9	CH ₃ OCH ₃
553 240.3	CH ₃ CN	555 126.8	CH ₃ OCH ₃	555 639.4	CH ₃ OCH ₃
553 362.2	CH ₃ CN	555 127.3	CH ₃ OCH ₃	555 639.8	CH ₃ OCH ₃
553 437.5	CH ₃ OH	555 128.2	CH ₃ OCH ₃	555 641.4	CH ₃ OCH ₃
553 570.9	CH ₃ OH	555 128.2	CH ₃ OCH ₃	555 641.4	CH ₃ OCH ₃
553 624.5	CH ₃ OH	555 129.1	CH ₃ OCH ₃	555 642.9	CH ₃ OCH ₃
553 667	U-line	555 204.1	SO ₂	555 666.3	SO ₂
553 681.3	³³ SO	555 249.8	CH ₃ OCH ₃	555 676.3	CH ₃ OCH ₃
553 707.6	CH ₃ CN	555 249.8	CH ₃ OCH ₃	555 676.3	CH ₃ OCH ₃
553 716	U-line	555 251.3	CH ₃ OCH ₃	555 678.3	CH ₃ OCH ₃
553 763.7	CH ₃ OH	555 252.3	CH ₃ OCH ₃	555 679.9	CH ₃ OCH ₃
554 052.7	CH ₃ OH	555 252.7	CH ₃ OCH ₃	555 680.3	CH ₃ OCH ₃

Table B.1. continued.

Frequency [MHz]	Molecule or U/T-line	Frequency [MHz]	Molecule or U/T-line	Frequency [MHz]	Molecule or U/T-line
555 681.0	CH ₃ OH	556 212.0	CH ₃ OCH ₃	561 138.5	¹³ CH ₃ OH
555 681.9	CH ₃ OCH ₃	556 212.1	CH ₃ OCH ₃	561 265.6	SO ₂
555 681.9	CH ₃ OCH ₃	556 212.2	CH ₃ OCH ₃	561 269.1	CH ₃ OH
555 683.6	CH ₃ OCH ₃	556 267	T-line	561 361.4	SO ₂
555 700.1	¹³ CH ₃ OH	556 594.4	CH ₃ OH	561 392.9	SO ₂
555 707.6	CH ₃ OCH ₃	556 603.7	CH ₃ OH	561 402.9	CH ₃ OH
555 707.6	CH ₃ OCH ₃	556 633	T-line	561 490.5	SO ₂
555 709.7	CH ₃ OCH ₃	556 936.0	<i>ortho</i> -H ₂ O	561 560.3	SO ₂
555 711.4	CH ₃ OCH ₃	556 959.9	SO ₂	561 608.6	SO ₂
555 711.8	CH ₃ OCH ₃	557 115.2	CH ₃ OH	561 639.3	SO ₂
555 713.5	CH ₃ OCH ₃	557 123.2	H ₂ CS	561 656.7	SO ₂
555 713.5	CH ₃ OCH ₃	557 147.0	CH ₃ OH	561 664.2	SO ₂
555 715.2	CH ₃ OCH ₃	557 147.0	CH ₃ OH	561 700.4	³⁴ SO
555 731.2	CH ₃ OCH ₃	557 184.4	²⁹ SiO	561 712.8	C ¹⁷ O
555 731.2	CH ₃ OCH ₃	557 283.2	SO ₂	561 789.7	CH ₃ OH
555 733.4	CH ₃ OCH ₃	557 676.6	CH ₃ OH	561 899.3	H ₂ CO
555 735.2	CH ₃ OCH ₃	558 004.6	CH ₃ OH	561 971	U-line
555 735.5	CH ₃ OCH ₃	558 087.7	SO	562 118	T-line
555 737.3	CH ₃ OCH ₃	558 101.2	SO ₂	562 960	U-line
555 737.3	CH ₃ OCH ₃	558 276.8	CH ₃ OH	563 033	U-line
555 739.1	CH ₃ OCH ₃	558 344.5	CH ₃ OH	563 481	T-line
555 748.2	CH ₃ OCH ₃	558 390.9	SO ₂	564 105	U-line
555 748.2	CH ₃ OCH ₃	558 555.8	SO ₂	564 221.6	CH ₃ OH
555 750.5	CH ₃ OCH ₃	558 606.4	CH ₃ OH	564 223.7	¹³ CH ₃ OH
555 752.3	CH ₃ OCH ₃	558 717.5	³⁴ SO ₂	564 249.2	SiO
555 752.7	CH ₃ OCH ₃	558 812.5	SO ₂	564 418	T-line
555 754.6	CH ₃ OCH ₃	558 890.2	CH ₃ OH	564 418	T-line
555 754.6	CH ₃ OCH ₃	558 890.2	CH ₃ OH	564 759.8	CH ₃ OH
555 754.6	CH ₃ OCH ₃	558 890.2	CH ₃ OH	565 245.2	¹³ CH ₃ OH
555 756.4	CH ₃ OCH ₃	558 904.6	CH ₃ OH	565 262.1	CH ₃ OCH ₃
555 759.7	CH ₃ OCH ₃	558 914.0	CH ₃ OH	565 262.8	CH ₃ OCH ₃
555 759.7	CH ₃ OCH ₃	558 966.6	N ₂ H ⁺	565 265.2	CH ₃ OCH ₃
555 762.1	CH ₃ OCH ₃	558 990.5	OCS	565 267.9	CH ₃ OCH ₃
555 764.0	CH ₃ OCH ₃	559 239	U-line	565 267.9	CH ₃ OCH ₃
555 764.0	CH ₃ OCH ₃	559 239	U-line	565 527.8	¹³ CH ₃ OH
555 764.4	CH ₃ OCH ₃	559 319.8	SO	565 737.4	¹³ CH ₃ OH
555 766.3	CH ₃ OCH ₃	559 500.4	SO ₂	565 737.4	¹³ CH ₃ OH
555 766.3	CH ₃ OCH ₃	559 586.1	CH ₃ OH	565 857.5	HDCO
555 766.8	CH ₃ OCH ₃	559 816	T-line	565 895.0	¹³ CH ₃ OH
555 766.8	CH ₃ OCH ₃	559 861	U-line	565 914.4	¹³ CH ₃ OH
555 768.2	CH ₃ OCH ₃	559 882.1	SO ₂	565 946.2	¹³ CH ₃ OH
555 769.2	CH ₃ OCH ₃	559 913	U-line	566 046.6	CH ₃ OCH ₃
555 771.2	CH ₃ OCH ₃	560 178.7	SO	566 047.3	CH ₃ OCH ₃
555 771.6	CH ₃ OCH ₃	560 291.0	CH ₃ OH	566 049.3	CH ₃ OCH ₃
555 773.5	CH ₃ OCH ₃	560 318.9	SO ₂	566 051.7	CH ₃ OCH ₃
555 773.5	CH ₃ OCH ₃	560 590.2	³⁴ SO ₂	566 066	U-line
555 775.5	CH ₃ OCH ₃	560 613.5	SO ₂	566 066	U-line
555 914	T-line	560 613.5	SO ₂	566 411.9	¹³ CH ₃ OH
555 933	T-line	560 648.9	CH ₃ OCH ₃	566 606.7	CH ₃ OCH ₃
556 115.8	CH ₃ OH	560 648.9	CH ₃ OCH ₃	566 606.7	CH ₃ OCH ₃
556 179.4	CH ₃ OCH ₃	560 648.9	CH ₃ OCH ₃	566 608.5	CH ₃ OCH ₃
556 179.4	CH ₃ OCH ₃	560 649.0	CH ₃ OCH ₃	566 610.4	CH ₃ OCH ₃
556 179.4	CH ₃ OCH ₃	560 649.0	CH ₃ OCH ₃	566 662.8	¹³ CH ₃ OH
556 179.4	CH ₃ OCH ₃	560 753	T-line	566 729.9	CN
556 179.5	CH ₃ OCH ₃	560 891.0	SO ₂	566 730.7	CN
556 212.0	CH ₃ OCH ₃	561 026.4	CH ₃ OH	566 730.8	CN
		561 094.8	SO ₂		

Table B.1. continued.

Frequency [MHz]	Molecule or U/T-line	Frequency [MHz]	Molecule or U/T-line
566 840.7	¹³ CH ₃ OH	570 303	U-line
566 946.8	CN	570 335	T-line
566 946.9	CN	570 619.0	CH ₃ OH
566 947.2	CN	570 624.2	¹³ CH ₃ OH
566 962.0	CN	570 790	T-line
566 963.7	CN	570 814	T-line
567 064.2	NO	571 119.7	OCS
567 069.6	NO	571 151	T-line
567 073.4	NO	571 217	T-line
567 077.9	NO	571 477	T-line
567 079.6	H ₂ S	571 532.6	SO ₂
567 082.7	NO	571 553.3	SO ₂
567 086.6	NO	572 112.8	¹⁵ NH ₃
567 485	U-line	572 498.2	NH ₃
567 592.7	SO ₂	572 596	U-line
567 942.6	CH ₃ OH	572 676.2	CH ₃ OH
568 050.7	H ₂ S	572 678	U-line
568 430.6	CH ₃ OCH ₃	572 898.8	CH ₃ OH
568 432.6	CH ₃ OCH ₃	573 471.1	CH ₃ OH
568 433.9	CH ₃ OCH ₃	573 527.3	³⁴ SO ₂
568 435.3	CH ₃ OCH ₃	573 912.7	CH ₃ OH
568 436.3	CH ₃ OCH ₃	574 090.9	CH ₃ OCH ₃
568 437.2	CH ₃ OCH ₃	574 090.9	CH ₃ OCH ₃
568 437.7	CH ₃ OCH ₃	574 093.3	CH ₃ OCH ₃
568 439.2	CH ₃ OCH ₃	574 095.7	CH ₃ OCH ₃
568 566.1	CH ₃ OH	574 140.0	H ₂ CS
568 690.1	CH ₃ OCH ₃	574 184	U-line
568 690.1	CH ₃ OCH ₃	574 587.8	SO ₂
568 690.3	CH ₃ OCH ₃	574 797.9	³⁴ SO ₂
568 690.4	CH ₃ OCH ₃	574 807.3	SO ₂
568 741.6	SO	574 868.5	CH ₃ OH
568 783.6	CH ₃ OH	575 397	T-line
568 999.3	CH ₃ CN	575 547.2	CH ₃ OH
569 091.6	³⁴ SO ₂	576 042.1	SO ₂
569 138	U-line	576 267.9	CO
569 324.5	CH ₃ OH	576 446	U-line
569 486.9	CH ₃ CN	576 708.3	H ₂ CO
569 606.3	CH ₃ CN	576 720.2	NS
569 704.0	CH ₃ CN	577 160	T-line
569 780.1	CH ₃ CN		
569 834.5	CH ₃ CN		
569 867.1	CH ₃ CN		
569 878.0	CH ₃ CN		
570 219.1	CH ₃ OCH ₃		
570 221.9	CH ₃ OCH ₃		
570 223.3	CH ₃ OCH ₃		
570 223.3	CH ₃ OCH ₃		
570 224.7	CH ₃ OCH ₃		
570 224.7	CH ₃ OCH ₃		
570 226.1	CH ₃ OCH ₃		
570 227.5	CH ₃ OCH ₃		
570 261.5	CH ₃ OH		
570 264.0	CH ₃ OH		